SCIENTIFIC REPORTS

OPEN

SUBJECT AREAS:
CNS CANCER
CANCER GENOMICS

Received
22 September 2014

Accepted
22 December 2014

Published
21 January 2015

Correspondence and requests for materials should be addressed to S.D. (sd1@nibmg.ac.in) or S.D. (Surajit_dhara@hotmail.com)

* These authors contributed equally to this work.

Variant allele frequency enrichment analysis *in vitro* reveals sonic hedgehog pathway to impede sustained temozolomide response in GBM

Nidhan K. Biswas[1]*, Vikas Chandra[1]*, Neeta Sarkar-Roy[1], Tapojyoti Das[1], Rabindra N. Bhattacharya[2], Laxmi N. Tripathy[3], Sunandan K. Basu[3], Shantanu Kumar[1], Subrata Das[1], Ankita Chatterjee[1], Ankur Mukherjee[1], Priyadarshi Basu[1], Arindam Maitra[1], Ansuman Chattopadhyay[4], Analabha Basu[1] & Surajit Dhara[1]

[1]National Institute of Biomedical Genomics, Kalyani, West Bengal 741251, India, [2]AMRI Hospitals, JC-16 Salt Lake City, Kolkata 700098, India, [3]Medica Superspeciality Hospital, 127 Mukundapur, Kolkata 700099, India, [4]University of Pittsburgh, 3550 Terrace Street, Pittsburgh, PA 15261, USA.

Neoplastic cells of Glioblastoma multiforme (GBM) may or may not show sustained response to temozolomide (TMZ) chemotherapy. We hypothesize that TMZ chemotherapy response in GBM is predetermined in its neoplastic clones via a specific set of mutations that alter relevant pathways. We describe exome-wide enrichment of variant allele frequencies (VAFs) in neurospheres displaying contrasting phenotypes of sustained versus reversible TMZ-responses *in vitro*. Enrichment of VAFs was found on genes ST5, RP6KA1 and PRKDC in cells showing sustained TMZ-effect whereas on genes FREM2, AASDH and STK36, in cells showing reversible TMZ-effect. Ingenuity pathway analysis (IPA) revealed that these genes alter cell-cycle, G2/M-checkpoint-regulation and NHEJ pathways in sustained TMZ-effect cells whereas the lysine-II&V/phenylalanine degradation and sonic hedgehog (Hh) pathways in reversible TMZ-effect cells. Next, we validated the likely involvement of the Hh-pathway in TMZ-response on additional GBM neurospheres as well as on GBM patients, by extracting RNA-sequencing-based gene expression data from the TCGA-GBM database. Finally, we demonstrated TMZ-sensitization of a TMZ non-responder neurosphere *in vitro* by treating them with the FDA-approved pharmacological Hh-pathway inhibitor vismodegib. Altogether, our results indicate that the Hh-pathway impedes sustained TMZ-response in GBM and could be a potential therapeutic target to enhance TMZ-response in this malignancy.

Glioblastoma multiforme (GBM) is a lethal malignancy of the central nervous system (CNS) showing dismal prognosis under the standard care of surgery, adjuvant radiotherapy and temozolomide (TMZ) chemotherapy[1]. Both radiotherapy and TMZ chemotherapy induce DNA damage in GBM neoplastic cells by means of generating double-strand breaks (DSB) and single-strand breaks (SSB) respectively. Ionizing radiation (IR) directly induces DSB and TMZ induces SSB by alkylating purine residues at the nucleotide positions of N-7, O-6 for Guanine (N-7-me-G, O-6-me-G) and N-3 for Adenine nucleotides (N-3-me-A), thus activating the base excision repair (BER) pathway[2–5]. Following alkylation, the damaged bases of the affected cells, are removed first by BER-glycosylase enzymes generating apurinic/apyrimidinic (AP)-sites followed by AP-endonucleases (APE) to finally generate SSB. Eventually both SSB and DSB converge to elicit the final response through common DNA damage response (DDR) pathways, to determine the fate of the damaged cell, either a sustained terminal response phenotype like apoptosis/senescence or a reversible response phenotype like quiescence (transient cell cycle arrest to repair the damage)[4,5]. Despite considerable knowledge of the molecular mechanism(s) of TMZ-response in GBM, it remains unclear why some cells respond to TMZ by showing a sustained effect such as apoptosis/cellular senescence while others do not.

A growing body of evidence *in vitro* as well as *in vivo* suggests clonal heterogeneity of cancer cells (genetic or non-genetic heterogeneity), to play a pivotal role in chemotherapy response[6–10]. We demonstrate here a plausible

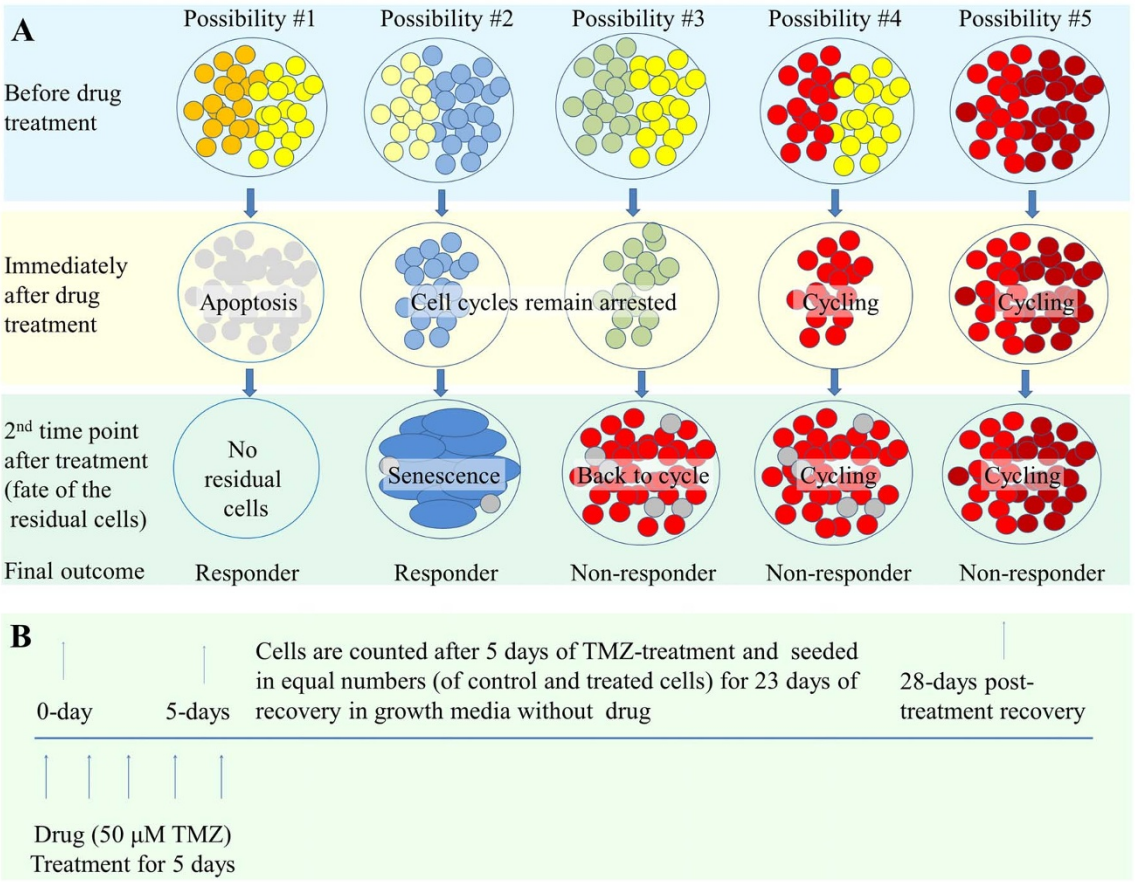

Figure 1 | (A) Schematic diagram of a model to explain TMZ-response in GBM neoplastic cells on the perspective of clonal heterogeneity. (**B**) The experimental design for TMZ-treatment and post-treatment recovery of GBM neurospheres *in vitro* to address this hypothetical model of TMZ-response.

model to explain TMZ-response of GBM neoplastic cells with the perspective of clonal heterogeneity. The most desirable outcome of GBM heterogeneous clones exposed to the maximum clinically achievable dose of TMZ[11] is induction of apoptosis and death. However, only a proportion of these clones induce apoptosis as an instant effect of TMZ-treatment. The residual clones, either show sustained growth arrest followed by induction of cellular senescence, or are non-responders. We sought to identify the genetic basis of these residual clones showing either a reversible drug-effect or a sustained drug-effect in response to TMZ. We explore here genetic heterogeneity of GBM neoplastic cells to estimate clonal enrichment in response to TMZ-treatment *in vitro*. Genetic heterogeneity assumes every individual clone to have a "signature set of mutations"[9,12]. Therefore, changes in clonal predominance after an exposure to chemotherapeutic drugs (*in vitro* or *in vivo*) will be reflected in the mutation spectrum of the cells as detected by comparison of variant allele frequencies (VAFs) before and after drug exposure[13].

We hypothesize TMZ-response to be predetermined in clones of GBM neoplastic cells with a specific set of mutations altering relevant pathways. In order to test the hypothesis, we developed an *in vitro* TMZ-treatment and post-treatment recovery model with GBM patient-derived neurospheres in our laboratory following a model previously described by Mihaliak *et al*,[14]. First we identified two clinical patients, one a TMZ-responder still living as of publication (for more than 38 months) and the other a non-responder who died within 3 months of surgery. Then we isolated neoplastic cells from surgically resected tumors from both patients, grew them in culture as neurospheres, exposed them to the maximum clinically achievable dose of TMZ (50 μM)[11] *in vitro* for 5 days, and then allowed them to grow for 28 days without the drug. Although the responder patient-derived neurosphere did not show induction of apoptosis in response to TMZ, almost all residual cells underwent TMZ-induced cellular senescence (TICS). Conversely, the non-responder patient-derived neurosphere underwent extensive apoptosis as an initial response to TMZ-treatment and the residual cells readily resumed proliferation upon drug withdrawal. These contrasting phenotypes were repeatedly observed in the two neurospheres irrespective of their cellular passages. In order to detect these two contrasting TMZ-responsive residual cells, we performed whole exome deep sequencing analysis of both the neurospheres at 3 different time points: before TMZ-treatment, after TMZ-treatment and after 28 days of post-treatment recovery *in vitro*. We then estimated exome-wide enrichment of VAFs and used Ingenuity pathway analysis (IPA) software to reveal the relevant pathways, as altered by the genes where VAFs were enriched in response to TMZ. Sonic hedgehog (Hh) pathway, one of the four pathways determined by our analysis, was significantly hyper-activated in cells showing reversible drug-effect. We then verified the likely involvement of the Hh-pathway by phenotypically clustering additional neurospheres in our repository with MGMT expression and TMZ-response *in vitro*. Finally, we demonstrated TMZ-sensitization of a TMZ-non-responder neurosphere *in vitro* by treatment with an FDA approved pharmacological Hh-pathway inhibitor vismodegib[15,16].

Results

A plausible model of chemotherapy response in GBM based on clonal heterogeneity. When GBM neoplastic cells are exposed to the chemotherapeutic drug TMZ, the first theoretical possibility (possibility # 1 in Fig. 1A) is that all cells undergo apoptosis and die, leaving no residual cells. Another extreme is possibility # 5 (Fig. 1A), nothing happens to the cells and they keep cycling. The other possibilities are partial apoptosis (possibilities #2, #3 and #4 in Fig. 1A). Under these

conditions, the residual cells following drug withdrawal may either show cell-cycle arrest (possibilities #2 and #3) or they may keep cycling (possibility #4). The cells which initially show cell-cycle arrest may either undergo a terminal differentiation by inducing cellular senescence resulting sustained response after the drug withdrawal (possibility #2) or may show reversible drug-effect by going back to the cell-cycle again (possibility #3). We provide evidence for possibilities #2 and #3 as a result of two GBM patient-derived neurospheres which repeatedly showed sustained versus reversible response to TMZ-treatment *in vitro*, irrespective of their cellular passages. Our experimental design of TMZ-treatment and post-treatment recovery (Fig 1B) was modified from Mihaliak *et al*,[14].

Clinical response of the two lead GBM patients. Clinical responses of the two lead GBM patients, from whom we identified the phenotypes, are briefly described here. The first patient A49910 was a TMZ-responder. Recurrence of the tumor along the periphery of the surgically resected area was revealed in this patient after the 2nd cycle of chemotherapy (Fig. 2c). This mass appeared to decrease in size as observed in the follow-up scans done 5 months later after the completion of all the 6 cycles of TMZ chemotherapy (Fig. 2d). This is suggestive of good response to TMZ chemotherapy. The patient appeared to be doing well and free from clinical progression during follow-up visits for more than 38 months post-surgery. The second patient M45481 died in three months after surgery despite a similar treatment regimen.

Development of GBM patient-derived neurospheres and MGMT analysis. We isolated neoplastic cells from tumors of GBM patients at the time of surgery and grew them in culture as neurospheres. Altogether six neurospheres were developed from tumor biopsies of six GBM patients (including the two lead patients as described above). Relative values of MGMT mRNA expression (relative to GAPDH mRNA) from all six tumor biopsy tissues and corresponding tumor-derived neurospheres, as given in Figures 2e and 2f respectively, showed a very tight correlation (Pearson r = 0.9513, p-value 0.0035). Henceforth, the isolated neurospheres will be referred as A49910, B0027, M45481, B0043, B0051 and B0048. MGMT expression in M45481 was significantly higher than that of A49910, both in tumor biopsy tissues (p-value 0.000243) and in the isolated neurospheres (p-value 9.71128e-05).

TMZ-treatment response of the isolated neurospheres *in vitro*. All the *in vitro* TMZ-treatment experiments were done on the neurospheres A49910 and M45481 between passages 4–16. Results were consistent in the neurospheres irrespective of their cellular passages *in vitro*. To simulate the 28-day cycle of TMZ chemotherapy in patients we treated all of the isolated neurospheres with the maximum clinically achievable dose of TMZ (50 μM) *in vitro* for 5 consecutive days and grew them for another 23 days without any drug intervention (post-treatment recovery). After 5 days, in A49910 viable cell count was 54.6 ± 22.9% (p-value 1.067e-05) and in M45481 it was 32.3 ± 6.6% (p-value 9.883e-07) compared to their

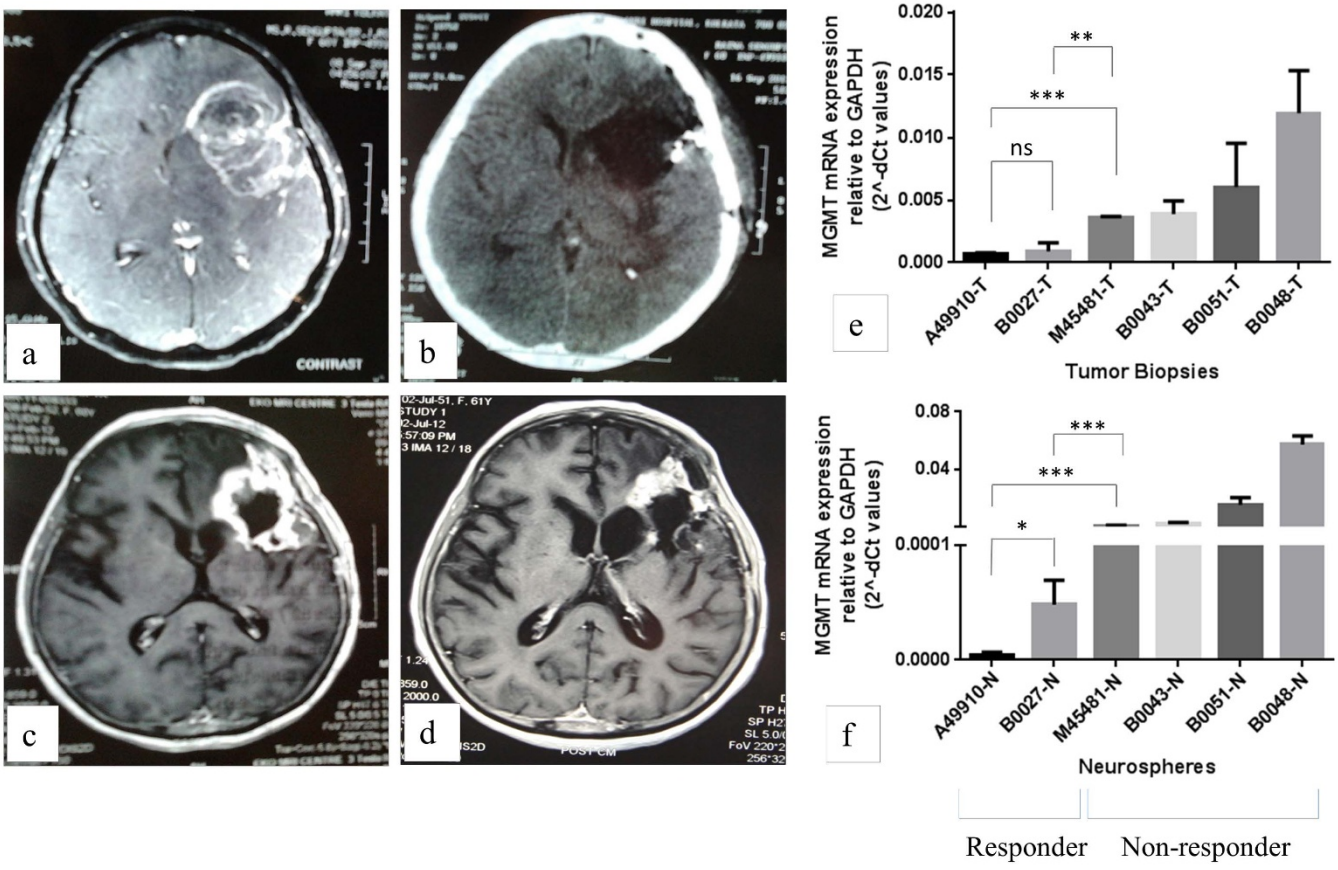

Figure 2 | Radiological images of responder GBM patient A49910 and MGMT mRNA expressions of 6 GBM patient-derived tumor biopsy tissues and isolated neurospheres. (**a**), Diagnostic MRI scan of the brain showing a space-occupying lesion (SOL) in insular cortex in A49910. (**b**), Postoperative CT scan showing gross total resection in A49910. (**c**), MRI scan image after the 2nd cycle of chemotherapy showing recurrence of the tumor in A49910. (**d**), Follow-up scan after 6 cycles of chemotherapy showing decrease in the size of the lesion in A49910. qRT-PCR estimation of MGMT mRNA expression relative to GAPDH mRNA expression in (**e**), GBM tumor biopsies and (**f**), in corresponding neurospheres isolated from the tumors. (* p-value < 0.05, ** p-value < 0.01 and *** p-value < 0.001).

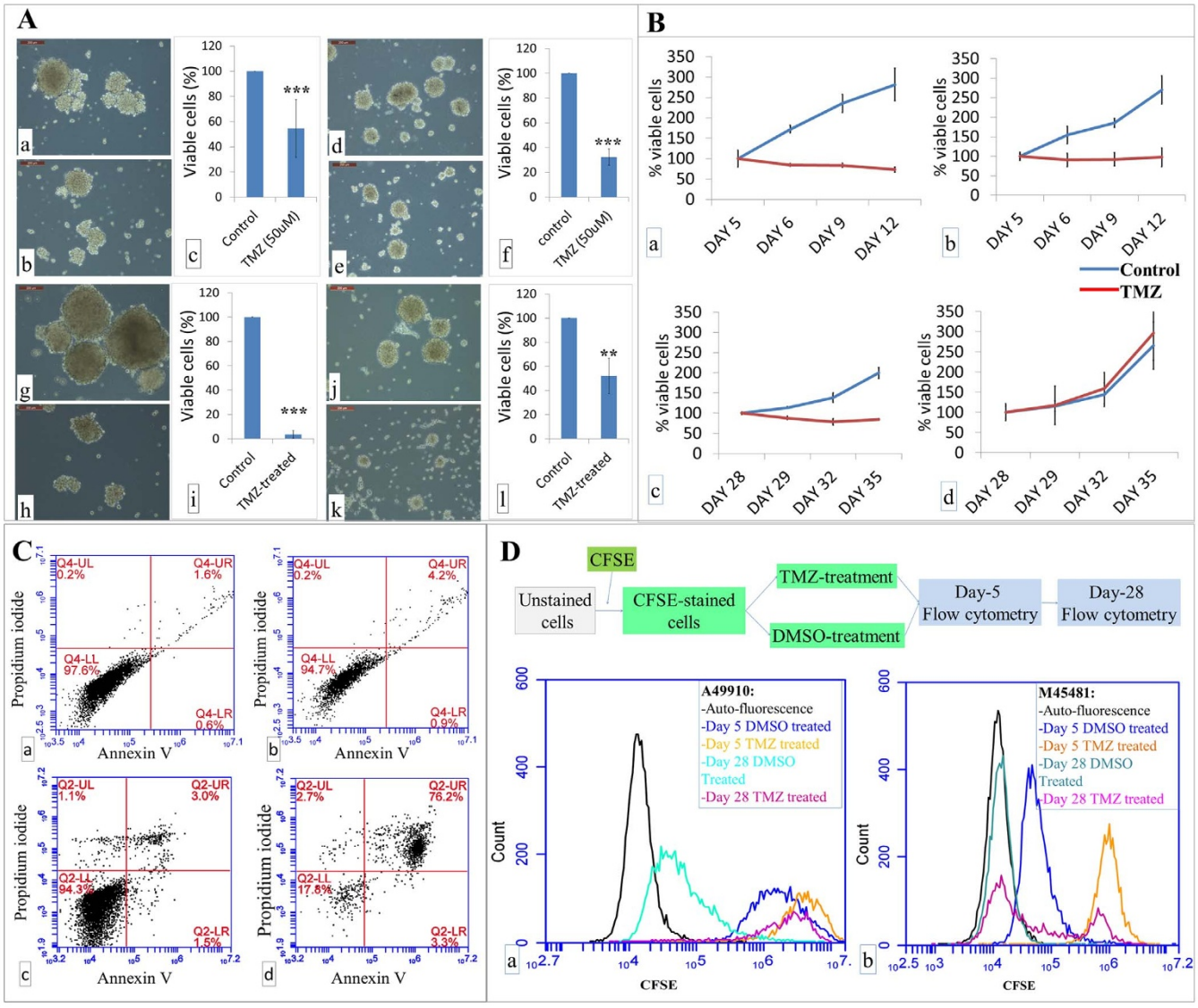

Figure 3 | (A) Light microscopic images (200 μm bar) and viable cell count of the neurospheres following TMZ treatment and post-treatment recovery. (**a**), DMSO treated control and (**b**), 5 days TMZ-treated neurospheres in A49910. (**c**), % viable cells in A49910 with DMSO- and 5 days of TMZ-treatment. (**d**), DMSO-treated control and (**e**), 5 days TMZ-treated neurospheres in M45481. (**f**), % viable cells in M45481 with DMSO- and 5 days of TMZ- treatment. (**g**), DMSO-treated control and (**h**), 28 days of post-TMZ-treated neurospheres in A49910. (**i**), % viable cells of DMSO-treated controls and 28 days of post-TMZ-treated cells in A49910. (**j**), DMSO treated control and (**k**), 28 days post-TMZ-treated neurospheres in M45481. (**l**), % viable cells of DMSO-treated controls and 28 days of post-TMZ-treated cells in M45481. (* p-value < 0.05, ** p-value < 0.01 and *** p-value < 0.001). (**B**) Growth curves (MTS assay) following 5 days of TMZ treatment and 28 days of post-treatment recovery. (**a**), A49910 DMSO-treated control and 5 days of TMZ-treated cells; (**b**), M45481 DMSO-treated control and 5 days of TMZ-treated cells; (**c**), A49910 DMSO-treated control and 28 days of post-TMZ-treated cells; (**d**), M45481 DMSO-treated control and 28 days of post-TMZ-treated cells. (**C**), flow cytometry analysis of apoptosis using annexin V and propidium iodide staining. (**a**), DMSO-treated A49910 cells, (**b**), 5 days of TMZ-treated A49910 cells, (**c**), DMSO treated M45481 cells and (**d**), 5 days of TMZ-treated M45481 cells. (**D**) Tracking cell division by CFSE staining. (**a**), growth arrest of TMZ-treated A49910 cells at day 5 of treatment (yellow line) compared to corresponding DMSO-treated control (blue line). The TMZ-treated A49910 cells remained arrested till day 28 post-treatment recovery (pink line) while the DMSO-treated control cells proliferated (green line). (**b**), Growth arrest in TMZ-treated M45481 cells at day 5 of treatment (yellow line) compared to corresponding DMSO-treated controls (blue line). At day 28 post-treatment recovery one subpopulation of TMZ-treated M45481 cells showed growth arrest while other subpopulation proliferated (pink line) showing a staining intensity almost similar to their corresponding DMSO-treated control cells (green line).

corresponding DMSO-treated controls (as 100%) as shown in Figure 3A c and f. But after 28th day the viable cell count was 3.5 ± 3.2% in A49910 (p-value1.231e-10) and 52.1 ± 14.6% in M45481 (p-value 0.001117) suggesting sustained effect of the drug only in A49910, but not in M45481 (Fig 3A i and l). TMZ-treatment experiments *in vitro* were repeated 6 times on A49910 and 3 times on M45481 with technical replicates. Error bars were generated and statistical significances (p-values) were calculated including all the independently repeated experiments as biological replicates.

Growth curves of the neurospheres following TMZ-treatment and post-treatment recovery. After 5 days of TMZ-treatment, both A49910 and M45481 cells showed significant growth inhibition compared to their respective DMSO-treated controls as shown in

Figures 3B a and b (p-values were 0.00028 for A49910 and 0.00191 for M45481 after 5 days of treatment). After 28th day of post-treatment recovery it was only the TMZ-treated cells of A49910 but not that of M45481 showed sustained growth retardation, as shown in Figures 3B c and d (p-values 0.00551 for A49910 and 0.35536 for M45481after 28 days of post-treatment recovery). Error bars were generated from the triplicate OD values of each experiment. All the MTS assays were repeated at least 2 times for each cell types at their two independent passages and found consistent results.

Apoptosis versus sustained growth arrest in response to TMZ-treatment. We observed extensive apoptosis in M45481 cells, as shown by 76% annexin V and propidium iodide double positive cells (Fig. 3C d), in response to 5 days of TMZ-treatment, whereas in A49910 it was only 4.2% (Fig. 3C b). On the other hand, A49910 cells showed sustained growth arrest till 28th day even after the drug withdrawal after 5 days, but the residual cells of M45481 resumed proliferation upon withdrawal of the drug as demonstrated by CFSE (Carboxy Fluorescein Succinimidyl Ester) staining (Fig. 3D a and b respectively). Corroborating with MTS assay (as described above) CFSE staining clearly demonstrated growth arrests in both A49910 and M45481 cells after 5 days of TMZ-treatment but that growth arrest was sustained till 28th day only in TMZ-treated cells of A49910, not that of M45481(pink lines in Figure 3D a and b respectively).

TMZ-induced cellular senescence (TICS) *in vitro*. Sustained growth arrest in A49910 is due to induction of cellular senescence as revealed by flattened cellular morphology and SA-β-Gal staining. Morphologies at the single cellular levels as repeatedly observed in all the *in vitro* TMZ-treatment experiments are represented in Figure 4A. At day 5, qualitatively, there were no morphological differences observed between the TMZ-treated cells of A49910 (Fig. 4A e) and their corresponding DMSO treated cells (Fig. 4A a) but at day 28, large and flattened appearance was visible only in the TMZ-treated cells (Fig. 4A f) but not in the corresponding DMSO-treated cells (Fig. 4A b). Unlike A49910, at day-5, the TMZ-treated cells of M45481 (Fig 4A g) were appearing slightly bigger than their corresponding DMSO-treated control cells (Fig 4A c) but at day 28, both the TMZ-treated (Fig. 4A h) and the DMSO-treated (Fig. 4A d) cells appeared almost similar in sizes. By a qualitative SA-β-Gal colorimetric staining, the TMZ-treated A49910 cells showed intense blue cytoplasmic staining of SA-β-Gal at day 28 post-treatment recovery (Fig. 4B f), suggesting induction of cellular senescence by TMZ-treatment. Some degree of blue cytoplasmic staining was also observed in DMSO-treated control cells of A49910 at day 28, but unlike the TMZ-treated cells, the control cells did not show any big and flat morphology. However, M45481 cells did not show any SA-β-Gal staining, neither after 5 days of TMZ-treatment (Fig. 4B c vs. g) nor after 28 days of post-treatment recovery (Fig. 4B d vs. h).

Enrichment of VAFs in response to TMZ-treatment and post-treatment recovery. From the phenotypes we see the residual cells of A49910 showing sustained growth arrest and TICS in response to TMZ-treatment *in vitro*. On the other hand, the residual cells of M45481 resume proliferation readily after the drug withdrawal, despite showing extensive apoptosis as an initial response to TMZ-treatment *in vitro*. In order to detect the "specific set of mutations" in the residual cells of both the neurospheres following TMZ-treatment we analyzed the exome-wide enrichment of VAFs locus by locus in both the neurospheres at 3 different time points – before TMZ treatment (C5), 5 days after TMZ treatment (T5) and 28 days after post-treatment recovery (T28). Significantly (p-values < 0.01) altered VAFs showed biphasic trends of change with the first phase representing the comparisons between C5 to T5 and the second phase between T5 to T28 as shown in Figure 4C. In this way altogether 77 loci were identified in A49910, of them 45 were enriching. Similarly, 92 loci were identified in M45481of them 51 were enriching. The enriching VAFs are shown in red arrows in Figure 4C. Lists of all these loci are given in Supplementary Tables S17A and S17B. Detailed lists of the variant loci showing these trends of VAF enrichment are given in Supplementary Tables S2 through S14.

Bioinformatic analyses of pathways by Ingenuity pathway analysis (IPA). Next we detected the pathways altered by the genes on which the variant loci (mutations) were enriching in response to TMZ-treatment *in vitro*. As shown in Table 1 cell-cycle G2/M DNA damage checkpoint regulation and double strand break repair by non-homologous end joining (NHEJ) were the two pathways altered in A49910 by genes with enriching VAFs – by PRKDC, encoding for the catalytic subunit of the DNA-dependent protein kinase (DNA-PKcs), and by RPS6KA1, encoding for a member of the RSK (ribosomal S6 kinase) family of serine/threonine kinases respectively. Similarly, the pathways altered in M45481 by the genes with enriching VAFs were lysine degradation II, V, phenylalanine degradation IV and sonic hedgehog (Hh) signaling pathway – altered by AASDH gene encoding for 2-Aminoadipic 6-Semialdehyde dehydrogenase enzyme and by STK36 gene encoding for an enzyme serine/threonine protein kinase 36 respectively. The selected list of genes where VAFs enriched $\geq$ 70% and/or the genes significantly altered relevant pathways as revealed by IPA are summarized in Table 1. The complete list of significantly altered pathways as revealed by IPA is given in Supplementary Table S16.

Functional validation of increased Hh-pathway activity (in the residual cells) through TMZ-treatment and post-treatment recovery. First by Sanger sequencing analysis we confirmed the presence of the variant locus of STK36 (Chromosome 2: 219557978 G to A) in M45481 but not in A49910 (Fig. 4D), taking two independent passages of each cell types. This mutation appeared to be novel. PolyPhen-2 prediction software showed it was a "deleterious" mutation (Supplementary Table S15) but we do not know at this moment how precisely this novel mutation on STK36 gene might be influencing the Hh-pathway activity in GBM. Therefore, we checked expressions of 11 canonical Hh-pathway component genes at three time points – before TMZ treatment, after TMZ treatment and after 28 days of post treatment recovery. As shown in Figure 4E a, mRNA expression of STK36 was found to be significantly increased in M45481 but not in A49910 cells upon TMZ-treatment. Significant increase in mRNA expressions was observed for the Hh-transcription factors GLI1, GLI2 and GLI3 upon TMZ-treatment and post-treatment recovery (Fig 4E b, c, d). Similar patterns were also observed for SNAI1, as a bona fide downstream target of the Hh-pathway, and for MGMT, as a bona fide covariate of TMZ response in GBM (Fig 4E e, f). These expression analyses were done in the neurospheres with biological replicates (at least 3 independently repeated experiments in each) as well as with the qRT-PCR technical replicates.

Validation on additional neurospheres for the likely involvement of Hh-pathway in TMZ-response. Next, we validated the likely involvement of Hh-pathway in TMZ-response on additional neurospheres from our repository. We estimated the expression correlations of MGMT – as a covariate for TMZ response – with the set of 11 Hh-pathway component genes on A49910, M45481, B0027, B0043, B0048 and B0051 neurospheres. As shown in Figure 5, MGMT expression correlated well with the expressions of GLI1 and SNAI1, in all the neurospheres only except in M45481. Unlike the other 5 neurospheres, expressions of GLI1/SNAI1 vs. MGMT were clearly discordant in this neurosphere. As shown in Figure 5 a, GLI1/SNAI1 expression in M45481 was as high as B0048 but MGMT expression was 61.3 fold lower than B0048. Therefore, we estimated expression correlation of the 11 Hh-pathway component genes with MGMT on the 5 neurospheres excluding M45481. For the rest of 5 neurospheres, A49910 and B0027 were responders whereas B0043, B0050 and

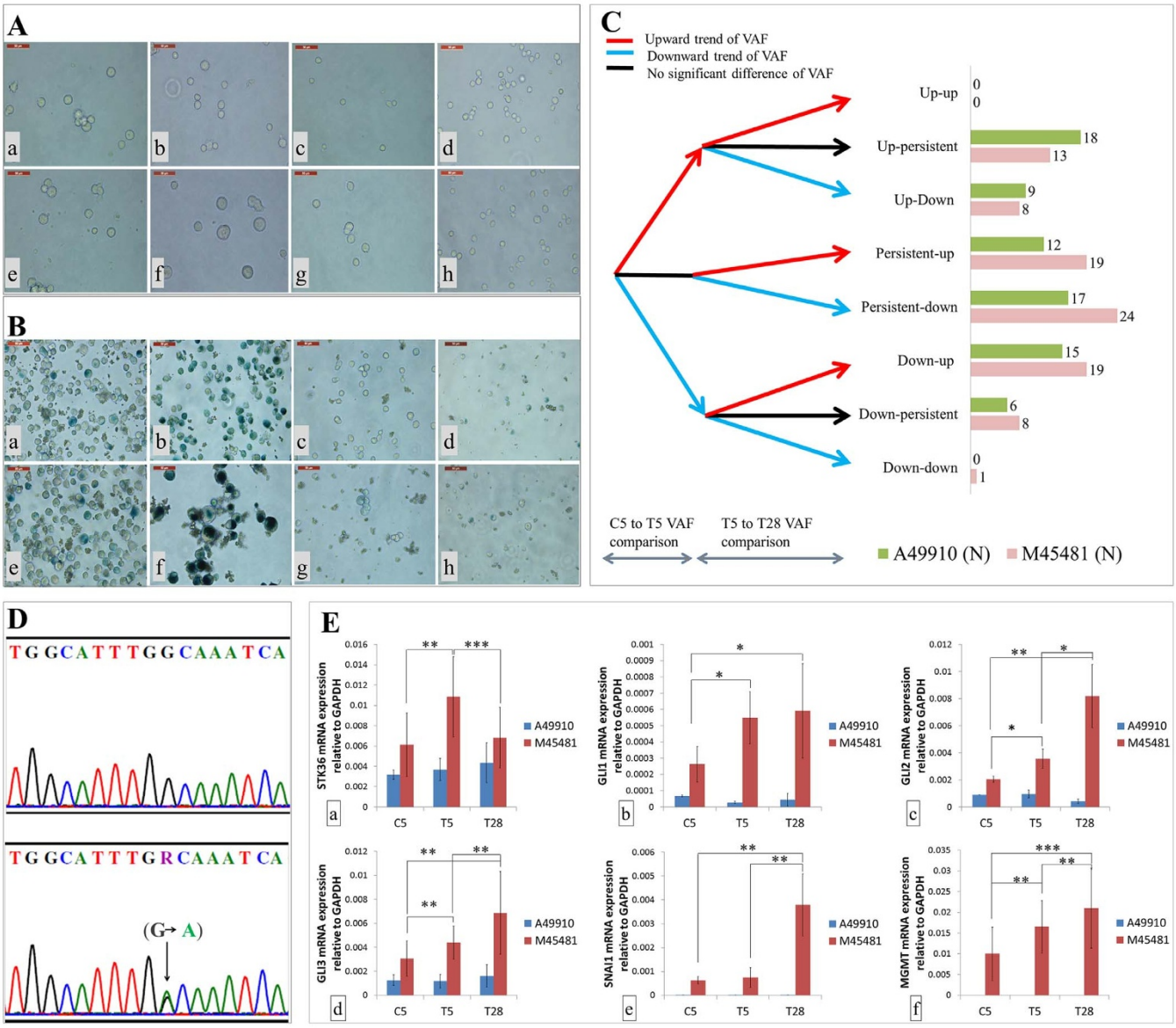

Figure 4 | (A) Light microscopic images (50 μm bar) at single cellular level. (**a**), day 5 DMSO-treated control cells of A49910, (**b**), day 28 DMSO-treated control cells of A49910. (**c**), day 5 DMSO-treated control cells of M45481, (d), day 28 DMSO-treated control cells of M4548, (**e**), day 5 TMZ-treated cells of A49910, (**f**), day 28 post-TMZ-treated cells of A49910, (**g**), day 5 TMZ-treated cells of M45481, and (**h**), day 28 post-TMZ-treated cells of M45481. (**B**) Light microscopic images (50 μm bar) of the cells showing SA-β-Gal staining following TMZ treatment and post-treatment recovery. (**a**), day 5 DMSO-treated control cells of A49910, (**b**), day 28 DMSO-treated control cells of A49910. (**c**), day 5 DMSO-treated control cells of M45481, (**d**), day 28 DMSO-treated control cells of M4548, (**e**), day 5 TMZ-treated cells of A49910, (**f**), day 28 post-TMZ-treated cells of A49910, (**g**), day 5 TMZ-treated cells of M45481, and (**h**), day 28 post-TMZ-treated cells of M45481. (**C**) VAFs showing biphasic trends where the first phase is the comparison of VAFs between C5 to T5 and second phase is the comparison of VAFs between T5 to T28. Red arrows are showing enriching VAFs in upward direction, blue showing downward direction and black showing no significant change. The green and purple horizontal bars on the right side represent the number of genes (N) in each category in A49910 and in M45481 respectively. (**D**) Sanger sequencing chromatogram showing a G to A transition on STK36 gene (arrow mark) in M45481 (lower panel) but not in A49910 (upper panel). (**E**) Showing mRNA expression patterns of Hh-pathway component genes, STK36 (**a**), GLI1 (**b**), GLI2 (**c**), GLI3 (**d**), Hh-pathway target gene SNAI1 (**e**) and MGMT (**f**) following TMZ-treatment and post-treatment recovery (C5, DMSO treated control; T5, day-5 TMZ-treated; T28, day-28 post-treatment recovery, *p-value < 0.05, **p-value < 0.01 and ***p-value < 0.001).

B0051 were non-responders as revealed by annexin V and CFSE staining experiments (data not shown). We found statistically significant correlations of expression of MGMT with that of the key component genes of the Hh-pathway GLI1 ($r = 0.9939$), SNAI1 ($r = 0.9917$) and SUFU ($r = 0.964$); ($|r| = 0.96$ is the 10% False Discovery Rate cutoff for significance). Linear regression of GLI1 on MGMT (Adjusted $R^2 = 0.9839$, p-value 0.00056) and that of SNAI1 on MGMT (Adjusted $R^2 = 0.9752$, p-value 0.008286), as in Figures 5 c and d respectively, suggest the Hh-pathway to be playing a significant role in TMZ-response of the GBM neurospheres.

Validation on TCGA-GBM database as a large clinical cohort of GBM. In order to further validate the correlations of expression of MGMT expression with that of GLI1 and SNAI1 on GBM patients, we downloaded TCGA-GBM RNA-Seq V2 database and extracted the whole transcriptomics data on 149 patients from the database[17]. mRNA expression of MGMT showed statistically significant correlation with that of SNAI1 (Spearman $r = 0.2678$, p-value 0.0010, $N = 149$) but surprisingly did not show significant (p-value 0.09) correlation with GLI1 (as given in the Supplementary Figure S1).

Table 1 | The selected list of genes where VAFs enriched above 70% and/or the genes significantly altered relevant pathways as revealed by IPA in A49910 and M45481.

Chromosome#	Locus	VAFs at C5	VAFs at T5	VAFs at T28	Hugo Symbol	Significantly altering pathways as detected by Ingenuity pathway analysis (IPA)
A49910						
11	8752598	72.73%	40%	94.74%	ST5	None
1	228494790	63.33%	50%	85.29%	OBSCN	None
1	11579470	30%	66.67%	78.79%	PTCHD2	None
7	91712698	70%	60%	77.50%	AKAP9	None
1	26883511	39.13%	37.50%	73.81%	RPS6KA1	Cell cycle G2/M DNA damage checkpoint regulation
10	37506700	50%	42.86%	72.22%	ANKRD30A	None
8	48798539	57.30%	35.82%	71.62%	PRKDC	Double strand break repair by non-homologous end joining
M45481						
13	39343807	52.38%	51.04%	76.54%	FREM2	None
17	56388238	68%	43.86%	73.33%	BZRAP1	None
6	116973182	60%	36.84%	70.83%	ZUFSP	None
4	57248716	35.44%	56.73%	42.37%	AASDH	Lysine II, V and phenylalanine degradation pathway
2	219557978	27.78%	16.54%	38.66%	STK36	Sonic hedgehog signalling pathway

TMZ-sensitization of a TMZ-non-responder neurosphere *in vitro* by Hh-pathway inhibitor vismodegib. However, in order to further understand the link between TMZ-response and the Hh-pathway in GBM we performed a proof of principle experiment *in vitro*. We performed this experiment on the most TMZ-resistant neurosphere (B0048) from our repository. As shown in Figure 6 a, b and the first two columns of e, there was no significant apoptosis induced by TMZ-treatment alone to this neurosphere *in vitro* (p-value 0.179). But a 3.2 fold increase (p-value 0.0004) in the total number of apoptotic cells in the same neurosphere was observed when the TMZ-treatment was done along with the FDA-approved Hh-pathway inhibitor drug vismodegib treatment *in vitro* (Fig. 6 e). Vismodegib treatment alone induced 2.2 fold (p-value 0.0011) apoptosis compared to the DMSO-treated control (Fig. 6 e). These results suggest the Hh-pathway could be a potential therapeutic target to enhance TMZ-response in this malignancy.

Discussion

To summarize, we have three major components to our study. First, we describe a model that explains varied TMZ-response of GBM. We observed the response of heterogeneous pool of GBM neoplastic cells treated with the maximum clinically achievable dose of the DNA-damaging chemotherapeutic agent TMZ *in vitro*. We determined that the residual cells demonstrated either sustained growth arrest followed by cellular senescence (in responder patient-derived neurosphere) or a transient cell-cycle arrest followed by a reversible drug-effect (in non-responder patient-derived neurosphere). Such reversible cell-cycle arrest by TMZ-treatment in GBM neurospheres *in vitro* was previously reported by Mihaliak *et al*,[14]. Induction of cellular senescence is recognized as an indicator of good TMZ-response in GBM[18] but not much is known about the mechanisms. TMZ chemotherapy in patients is given in 28-day cycles – 5 days of treatment and 23 days of recovery[1]. The later period allows patients to recover from the toxic effects of the drug and prepare for the next cycle, as do the neoplastic cells unless the drug effect is sustained in them. If GBM neoplastic cells do indeed show a sustained TMZ-effect via the induction of TICS during the recovery period, this could have a profound impact on the final outcome of TMZ chemotherapy. Suggesting, the fate of residual clones, either a sustained response or a reversible drug-effect following TMZ treatment, could be very important.

The second component of our study was to identify the genetic basis of residual clones demonstrating either TICS or reversible growth-arrest. We explored the genetic heterogeneity of the neurospheres in order to identify the "specific set of mutations" that are enriching in presence of TMZ *in vitro*. It is a long standing argument whether a resistant clone in a tumor is preexisting or generated *de-novo* by harsh treatment from a mutagenic or DNA damaging drug (such as TMZ). Regardless of origin, if a clone is altered upon TMZ exposure it will be reflected on the mutation spectrum by an enrichment of VAFs on loci throughout its genome. As we currently do not have a proper tool to address the dynamics of clonal heterogeneity, deep DNA sequencing technology is the only method which might be able to shed some light on this[13]. We used this method in TMZ-treated GBM neoplastic cells and found enrichment of VAFs on 45 genes in cells showing TICS (e.g., ST5, PRKDC and RPS6KA1) and on 51 genes in cells showing reversible TMZ-effect (e.g., FREM2, AASDH and STK36). These genes are relevant to the respective phenotypes observed in the two neurospheres. For instance, the A49910 neurosphere, which displayed flattened residual cell morphology, we found highest enrichment of VAF in the ST5 gene, which is involved in cytoskeletal reorganization[19]. Two genes enriched in the A49910 neurosphere following TMZ-treatment play central roles in the DNA damage response (DDR) pathways: PRKDC encodes for the catalytic subunit of the DNA-dependent protein kinase (DNA-PKcs), and RPS6KA1, encodes for a member of the RSK (ribosomal S6 kinase) family of serine/threonine kinases[20–22]. In the M45481 the highest enrichment of VAF was in FREM2, which encodes for an extracellular matrix component, associated with cellular migration and motility[23]. The M45481 also demonstrated lysine-II&V/phenylalanine degradation pathway via AASDH and sonic hedgehog (Hh) pathway via STK36[24,25]. The role of AASDH in cellular senescence/quiescence is not well defined, but amino acid degradation pathways in general can have significant impact on cell survival[26]. The Hh-pathway is a developmentally important signaling pathway known to be involved in proliferation, migration and survival of cancer cells[15,27,28]. All four signaling pathways detected by our analysis may be relevant to their respective phenotypes, but for the current study we selected the Hh-pathway for further validation experiments.

The third and last component of our study was validation. To begin, we confirmed the existence of the variant locus (G to A transition) on the STK36 gene by Sanger sequencing. The biological importance of this specific mutation on the STK36 gene is not yet clear to us at this moment. Serine/Threonine kinase STK36 alias "Fused (Fu)" is a key component of the Hh-pathway[24,25]. Experimentally knocking out this gene impairs the Hh-pathway activity but the kinase function of STK36 is not responsible for its key role in the Hh-pathway[24]. In a high throughput siRNA based functional assay[29], silencing of STK36 gene sensitizes established cultured cells to DNA damaging agents (PARP inhibitors), thereby suggesting its role in DDR. We

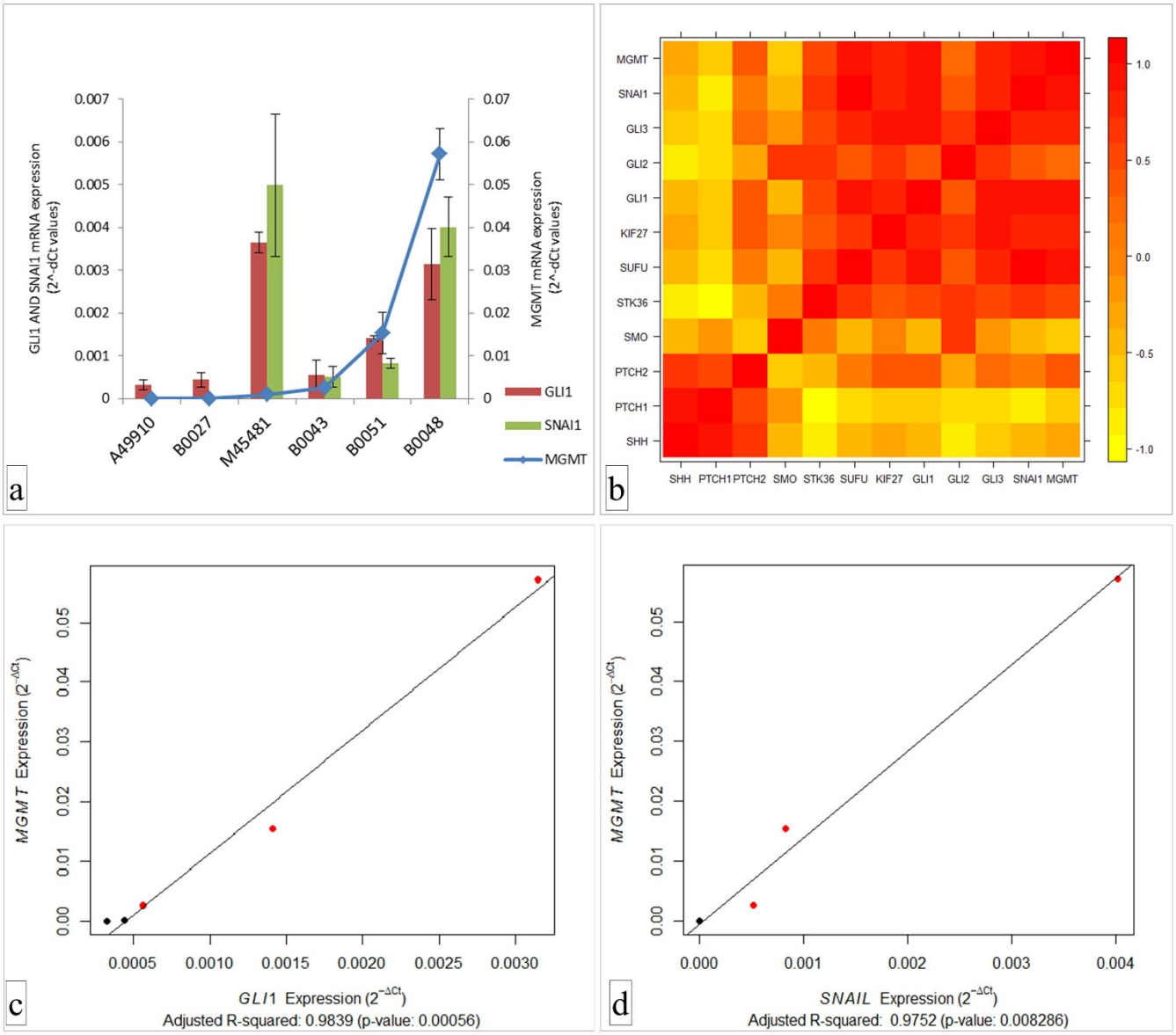

Figure 5 | (**a**), mRNA expressions of GLI1, SNAI1and MGMT in 6 neurospheres. (**b**), Correlation matrix of 11 Hh-pathway component genes and MGMT ($|r| = 0.96$ FDR 0.1) on 5 cells except M45481. (**c**), Regression model fitting with the expressions of GLI1 with MGMT and (**d**), SNAI1 with MGMT. Red dots representing non-responder cells and black dots responder cells.

observed a statistically significant increase of the Hh-pathway activity in response to DNA-damaging insult by TMZ in M45481 cells but not in A49910 cells. This also suggests an important role for the Hh-pathway in DDR.

For further validation using additional GBM neurospheres in our repository we selected MGMT as a covariate of TMZ-response[30,31] in order to estimate its expression correlation with the 11 canonical Hh-pathway component genes. They correlated well excluding the neurosphere M45481, which showed discordance in terms of MGMT and GLI1/SNAI1 expression patterns. The relative levels of GLI1/SNAI1 expressions in this neurosphere were as high as that of the most TMZ-resistant neurosphere B0048 but MGMT expression was 61.3 fold lower than B0048. However, despite being 61.3 fold lower than B0048, MGMT expression in M45481 neurosphere appeared to be more than 200 fold higher than that of the responder neurosphere A49910. Phenotypically, the neurosphere M45481 initially responded to TMZ-treatment *in vitro* but reverted back within 3–4 weeks of drug withdrawal. Therefore, in spite of showing an initial response to TMZ-treatment this neurosphere finally behaved like a non-responder. This "reversible non-response" phenotype was repeatedly observed in this neurosphere but we have no more such "reversible non-responder" neurospheres in our repository at this moment. Therefore, it could not be classified as a separate group and was excluded from this correlation analysis.

The patterns of MGMT expression in patient biopsy samples and in the neurospheres were tightly correlated. Interestingly, MGMT expression in the neurospheres of A49910, B0027 and M45481 was lower than in their corresponding tumor biopsies but it remained either unchanged in B0043 or even increased in B0048 and in B0051 neurospheres compared to their corresponding tumor biopsies. As further investigation was outside of our main area of study, we cautiously interpret these results as follows. Freshly resected tumor biopsy tissues can contain "non-tumor" cells, such as leukocytes, untransformed glial cells or even normal neurons. It is unlikely that MGMT is silenced in these normal cells, suggesting a relatively higher MGMT expression in biopsies (which is mixed up with normal cells) compared to the corresponding responder neurospheres. On the other hand, MGMT could be overexpressed in non-responder neurospheres

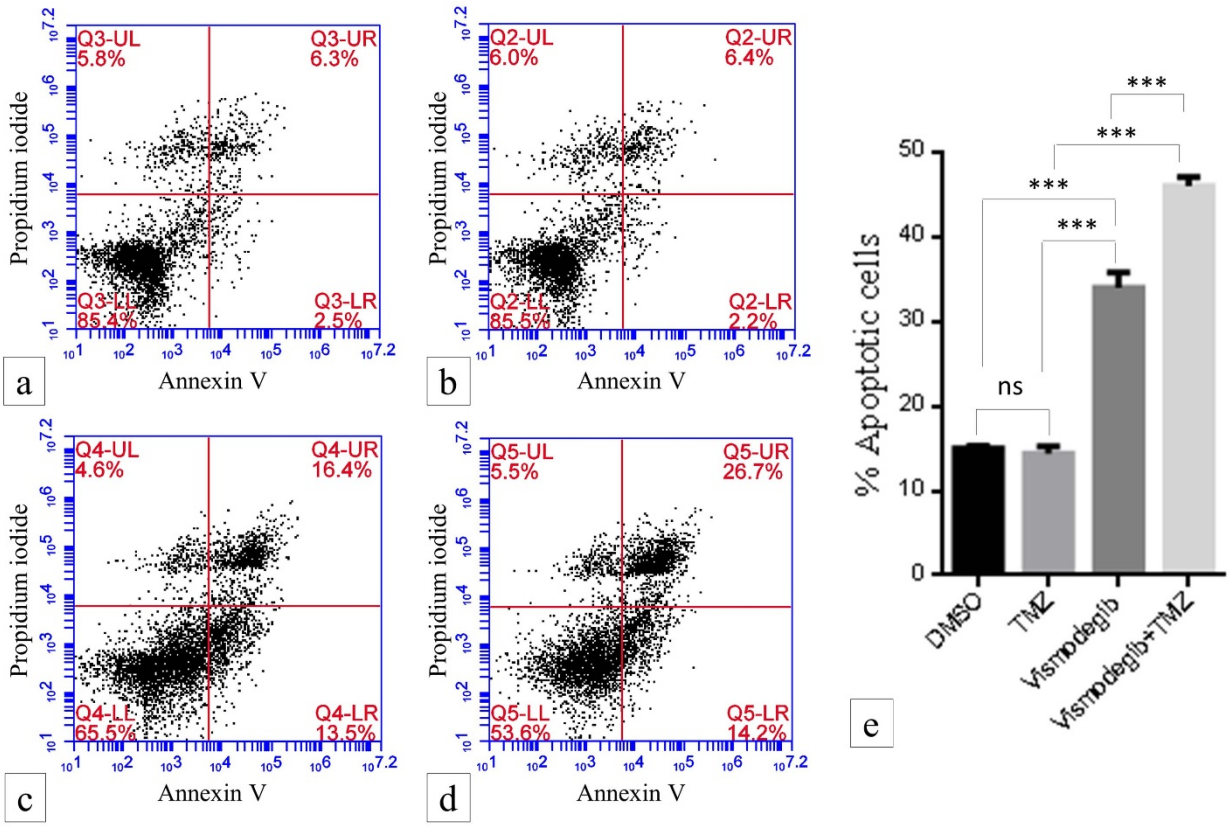

Figure 6 | Flow cytometry analysis of annexin-V and propidium iodide (PI) staining of apoptotic cells following vismodegib (50 μM) and TMZ (50 μM) treatment to B0048 neurosphere. a), DMSO-treated control, b), TMZ treatment alone, c) vismodegib treatment alone, d), TMZ treatment along with vismodegib treatment and e), showing % of apoptotic cells (annexin-V positive + PI positive + annexin-V and PI double positive cells). (* p-value < 0.05, ** p-value < 0.01 and *** p-value < 0.001).

compared to the normal cells. Therefore the resultant MGMT expression could be higher in the non-responder neurospheres compared to their corresponding tumor biopsies.

In our results MGMT expression was correlated with the expressions of GLI1 and SNAI, as well as with direct TMZ-response of these neurospheres *in vitro*. Although it is not a direct measure, MGMT expression is the closest measure of TMZ-response in GBM. Therefore we further tested the correlation of expression of MGMT with that of GLI1 and SNAI1 in the TCGA-GBM database with partial validation. MGMT expression was significantly correlated with SNAI1 but poorly correlated with GLI1. This indicates the possible influence of Hh-pathway intermediate factor (s) or co-factor (s) in GBM *in vivo* which could be a subject of further investigation. Finally, as a proof of principle experiment *in vitro* we demonstrated TMZ-sensitization of a TMZ-resistant neurosphere by treatment with the FDA approved pharmacological Hh-pathway inhibitor vismodegib. That is encouraging from the translational point of view and subject to a separate investigation including more *in vitro* experiments and preclinical mouse models.

The role of the Hh-pathway is known in various aspects of cancer cell biology but its role in chemoresistance is unclear. Recently, mechanistic details of how Hh-transcription factor GLI1 and SNAI1 impart chemoresistance in Acute Myeloid Leukemia (AML) have been explained[32]. Moreover, inhibition of the Hh-pathway together with the PI3K pathway is a better therapeutic option than inhibition of PI3K alone[33]. Precise mechanistic details of how Hh-pathway confers TMZ chemoresistance in GBM are currently being explored in our laboratory. In the present paper we demonstrated an *in vitro* model of clonal enrichment analysis by exome wide enrichment of VAFs in response to TMZ-treatment and post-treatment recovery. The TMZ-treatment and post-recovery model *in vitro* was shown before by Mihaliak *et al*,[14] and we have utilized this model to further understand the genetic basis of the residual clones showing sustained versus reversible TMZ-effect. To our understanding this is a first study of this kind where genetic heterogeneity of GBM neurospheres in response to TMZ *in vitro* has been explored as a discovery scale experiment to find out the genes and pathways responsible for TMZ-response. With this analysis we found the Hh-pathway to hinder sustained TMZ-response in GBM neoplastic cells. Therefore, there is a strong possibility of induction of apoptosis/cellular senescence in GBM neoplastic cells if the Hh-pathway is kept suppressed while treating GBM with TMZ. Clinically, inhibition of this pathway could be a potential strategy to enhance sustained TMZ-response in this malignancy.

Methods

Patient follow-up in clinic. Following the guidelines of the Declaration of Helsinki, all patients provided written consent in compliance with institutional review board (IRB) approvals from their respective institutes and hospitals. All methods were carried out in accordance with the NIBMG, India, Ethical Committee approved guidelines. Details of the patients' clinical follow-up information are given in the Supplementary Information.

Collection of tumor tissues and isolation of neurospheres. Fresh tumor tissues were collected from Operation Theater immediately after surgery. We utilized approximately 0.2 to 0.5 centimeter (~ size of a pencil eraser) sizes of resected tumors from patients to make single cell suspensions in order to develop neurospheres. Single-cell suspensions from tumor tissues were made by enzymatic digestion with Liberase selection grade (Roche Diagnostics GmbH, Germany, cat# 114106). The suspensions were treated with RBC lysis buffer for 5 minutes at room temperature. Then the suspensions were washed two times with ice cold PBS (1X) and finally the cell pellets were re-suspended and seeded with StemPro® NSC SFM media (Invitrogen, NY, USA cat# A10509-01) at standard mammalian tissue culture conditions to grow them as neurospheres. Approximately 4–5 million viable cells (as counted by trypan blue exclusion test at the final step) were seeded in 4ml of media in

a T-25 flask for developing neurospheres. We isolated 6 neurospheres A49910, M45481, B0027, B0043, B0048 and B0051 for our current study.

TMZ treatment to the neurospheres *in vitro*. Patient-derived neurospheres were treated with either 50 μM TMZ (Sigma-Aldrich, MO, USA cat# 76899) or with 0.1% DMSO (as vehicle control) for 5 days. Then the drug was withdrawn and the neurospheres were further grown for 23 days without drug. At the end of 5 days and 28 days they were trypsinized into single-cell suspensions and viable cell numbers were determined by hemocytometer following a standard trypan blue exclusion test. All images of the neurospheres and single cells were documented with inverted microscope Leica DM IL LED using the software Leica Application Suite Version 3.7.0 (Leica Microsystems GmbH, Germany,).

Growth curve analysis of neurospheres by MTS assay. Growth curve was determined by standard MTS assay using CellTiter 96^{R} AQueous One Solution Cell Proliferation Assay System (Promega Corporation, WI, USA cat# G3580) following manufacturer's protocol. MTS assay was done in triplicates at 4 different time points (0th, 1st, 3rd and 5th day) after 5 days of treatment and 28 days of post-treatment recovery.

Tracking cell division for 28 days by CFSE staining. Single cell suspensions of neurospheres were stained with Carboxyfluorescein succinimidyl ester (CFSE) using CellTrace™ CFSE Cell Proliferation Kit (Life technologies, Oregon, USA cat# C34554) following manufacturer's protocol. The stained cells were divided into two equal parts, one part treated with DMSO and the other part was treated with 50 μM TMZ for 5 days. CFSE staining intensities were measured by flow cytometry (BD Acuri™ C6, BD BioSciences, USA) after 5 days of treatment and at 28 days of post-treatment recovery.

Senescence associated β-Gal (SA-β -Gal) staining. SA-β-gal staining was done to determine cellular senescence using cellular senescence assay kit (Chemicon International, MA, USA cat # KAA002) following manufacturer's protocol. Briefly, approximately 5×10^5 cells were washed with 1x PBS, fixed by fixing solution provided with the kit, stained overnight with 2 ml freshly prepared 1x SA-β-gal detection solution and observed under phase contrast microscopy.

DNA/RNA extraction and quantitative reverse transcriptase polymerase chain reaction (qRT-PCR) analysis. All DNA and RNA were extracted from cells using AllPrep DNA/RNA Mini Kit (Qiagen GmbH, Germany cat# 80204). Reverse transcription was done using High Capacity cDNA Reverse Transcription Kit (Applied Biosystems, UK cat# 4368814) Quantitative measurements of target gene expression relative to either β-Actin or 18s RNA or GAPDH were performed in triplicates using Power SYBR Green PCR Master Mix (Applied Biosystems, UK cat# 4368706) following the manufacturer's recommendations in an ABI 7900HT Fast Real Time PCR system. Relative expression was defined by $2^{-\Delta Ct}$ method[34]. Error bars were generated from the triplicate $^{-\Delta Ct}$ values. The primer sequences are given in the Supplementary Table S18.

Whole exome sequencing (WES) experiments. Libraries for WES were constructed and sequenced on an Illumina HiSeq2000 using 100 bp paired-end reads following manufacturer's guidelines. Image analysis and base calling were performed using the Illumina Real Time Analysis (RTA) Pipeline version 1.12 with default parameters as previously reported[35]. Details of the experiments are given in Supplementary Information.

Analysis of variant allele frequency (VAF). VAF at a locus was defined as the proportion of the variant allele observed by the total depth at that position. Difference in VAF was measured using standardized two-sample *Z* Statistic. If p_{t1} be the VAF at a locus at time t_1 [t_1 *can be Day5 control (C5), Day5 TMZ-treated (T5) and Day 28 post-treatment recovery (T28)]* with depth n_1 and p_{t2} be the VAF for the same locus at a different time point t_2 (t_2 *can be C5, T5 and T28 but not* t_1) with depth n_2, the standardized Z Statistic with asymptotically normal properties is defined as

$$Z = \frac{p_{t1} - p_{t2}}{\sqrt{(p(1-p))\left[\frac{1}{n_1} - \frac{1}{n_2}\right]}} \text{ where, } p = (n_1 p_2 + n_2 p_2)/(n_1 + n_2).$$

We ranked all the significantly different VAFs based on their Z^2 values and preselected the top 1% in order to reduce false positive results.

Bioinformatic analyses of significantly altered pathways. Significantly over-represented pathways were identified using Ingenuity Pathway Analysis (IPA) web based application (accessed on 1st Aug, 2013). We downloaded the RNA-Seq based whole transcriptomics data available as open access (https://tcga-data.nci.nih.gov/tcga/accessed on May 20th 2014) and extracted gene expression results of the already published TCGA-GBM clinical cohort[17].

TMZ-sensitization of a TMZ non-responder neurosphere by inhibition of Hh-pathway *in vitro*. For this experiment we preselected a non-responder neurosphere from our repository (B0048) which was the most resistant to TMZ-treatment *in vitro*. We treated the cells either with maximum clinically achievable dose (50 μM) of vismodegib (Selleckchem, Houston, TX, USA, cat # S1082) or DMSO (0.1%) as placebo consecutively for 5 days. After 5 days both the DMSO-treated cells and vismodegib-treated cells were sub-divided into two parts. One part was treated with TMZ (50 μM) and the other part was continued with DMSO treatment. Similarly, the one part of the vismodegib-treated cells was treated with TMZ (50 μM) along with vismodegib (50 μM) and the other part was continued with vismodegib treatment alone. Annexin-V and propidium iodide staining was done on the cells after this complete course of treatment (altogether for 10 days). The number of apoptotic cells in each treatment was detected by flow cytometry analysis (BD Acuri™ C6, BD BioSciences, USA). The data presented as the total number of apoptotic cells in each treatment. The whole experiment was done in triplicate and the error bars were calculated from the independently repeated experiments.

Statistical analyses. To compare the differences in viable cell numbers of DMSO- and TMZ- treated cells, for the i^{th} set of experiments, we translated the number of viable TMZ-treated cells as percentage of viable DMSO-treated cells (u_i). The mean of u_i was compared with 100, using univariate t-test. Student's t-test was used to compare the gene expressions by quantitative RT-PCR experiments. We fitted a linear regression to approximate the growth curve by MTS assays. Days were taken as the independent variable (0, 1, 3, and 5) and OD values of MTS assays as dependent variable. For each cell two separate regressions were fitted using the control and the TMZ treated OD values. The slope of these two regression equations were compared both in day 5 and in day 28. Pearson's correlation coefficients (r) were determined on the expression of 11 canonical Hh-pathway component genes and MGMT in the neurospheres. Multiple testing correction was done with a False Discovery Rate[36] of 10%, to find out significant correlations. All statistical analyses were done using R 3.1 (http://www.r-project.org) and GraphPad Prism 6 (http://www.graphpad.com).

1. Stupp, R. *et al.* Radiotherapy plus concomitant and adjuvant temozolomide for glioblastoma. *The New England journal of medicine.* **352**, 987–996 (2005).
2. Hoeijmakers, J. H. DNA damage, aging, and cancer. *The New England journal of medicine* **361**, 1475–1485 (2009).
3. Denny, B. J., Wheelhouse, R. T., Stevens, M. F., Tsang, L. L. & Slack, J. A. NMR and molecular modeling investigation of the mechanism of activation of the antitumor drug temozolomide and its interaction with DNA. *Biochemistry.* **33**, 9045–9051 (1994).
4. Roos, W. P. & Kaina, B. DNA damage-induced cell death by apoptosis. *Trends in molecular medicine* **12**, 440–450 (2006).
5. Ciccia, A. & Elledge, S. J. The DNA damage response: making it safe to play with knives. *Molecular cell.* **40**, 179–204 (2010).
6. Shipitsin, M. *et al.* Molecular definition of breast tumor heterogeneity. *Cancer cell.* **11**, 259–273 (2007).
7. Brock, A., Chang, H. & Huang, S. Non-genetic heterogeneity--a mutation-independent driving force for the somatic evolution of tumours. *Nat Rev Genet.* **10**, 336–342 (2009).
8. Marusyk, A., Almendro, V. & Polyak, K. Intra-tumour heterogeneity: a looking glass for cancer? *Nature reviews.* **12**, 323–334 (2012).
9. Almendro, V., Marusyk, A. & Polyak, K. Cellular heterogeneity and molecular evolution in cancer. *Annual review of pathology.* **8**, 277–302 (2013).
10. Patel, A. P. *et al.* Single-cell RNA-seq highlights intratumoral heterogeneity in primary glioblastoma. *Science (New York, N.Y.* **344**, 1396–1401 (2014).
11. Newlands, E. S. *et al.* Phase I trial of temozolomide (CCRG 81045: M&B 39831: NSC 362856). *British journal of cancer.* **65**, 287–291 (1992).
12. Shackleton, M., Quintana, E., Fearon, E. R. & Morrison, S. J. Heterogeneity in cancer: cancer stem cells versus clonal evolution. *Cell.* **138**, 822–829 (2009).
13. Aparicio, S. & Caldas, C. The implications of clonal genome evolution for cancer medicine. *The New England journal of medicine.* **368**, 842–851 (2013).
14. Mihaliak, A. M. *et al.* Clinically relevant doses of chemotherapy agents reversibly block formation of glioblastoma neurospheres. *Cancer letters.* **296**, 168–177 (2010).
15. Amakye, D., Jagani, Z. & Dorsch, M. Unraveling the therapeutic potential of the Hedgehog pathway in cancer. *Nature medicine.* **19**, 1410–1422 (2013).
16. Axelson, M. *et al.* U.S. Food and Drug Administration approval: vismodegib for recurrent, locally advanced, or metastatic basal cell carcinoma. *Clin Cancer Res.* **19**, 2289–2293 (2013).
17. Brennan, C. W. *et al.* The somatic genomic landscape of glioblastoma. *Cell.* **155**, 462–477 (2013).
18. Chitikova, Z. V. *et al.* Sustained activation of DNA damage response in irradiated apoptosis-resistant cells induces reversible senescence associated with mTOR downregulation and expression of stem cell markers. *Cell cycle (Georgetown, Tex.* **13**, 1424–1439 (2014).
19. Hubbs, A. E., Majidi, M. & Lichy, J. H. Expression of an isoform of the novel signal transduction protein ST5 is linked to cell morphology. *Oncogene.* **18**, 2519–2525 (1999).
20. Roukos, V. *et al.* Spatial dynamics of chromosome translocations in living cells. *Science (New York, N.Y.* **341**, 660–664 (2013).
21. Novotna, E. *et al.* DNA-dependent protein kinase and its inhibition in support of radiotherapy. *International journal of radiation biology.* **89**, 416–423 (2013).
22. Houslay, M. D. A RSK(y) relationship with promiscuous PKA. *Sci STKE.* **2006**, pe32 (2006).
23. Timmer, J. R., Mak, T. W., Manova, K., Anderson, K. V. & Niswander, L. Tissue morphogenesis and vascular stability require the Frem2 protein, product of the

mouse myelencephalic blebs gene. *Proceedings of the National Academy of Sciences of the United States of America.* **102**, 11746–11750 (2005).
24. Murone, M. *et al.* Gli regulation by the opposing activities of fused and suppressor of fused. *Nature cell biology.* **2**, 310–312 (2000).
25. Wilson, C. W. *et al.* Fused has evolved divergent roles in vertebrate Hedgehog signalling and motile ciliogenesis. *Nature.* **459**, 98–102 (2009).
26. Struys, E. A. & Jakobs, C. Metabolism of lysine in alpha-aminoadipic semialdehyde dehydrogenase-deficient fibroblasts: evidence for an alternative pathway of pipecolic acid formation. *FEBS letters.* **584**, 181–186 (2010).
27. Feldmann, G. *et al.* Blockade of hedgehog signaling inhibits pancreatic cancer invasion and metastases: a new paradigm for combination therapy in solid cancers. *Cancer research.* **67**, 2187–2196 (2007).
28. Karhadkar, S. S. *et al.* Hedgehog signalling in prostate regeneration, neoplasia and metastasis. *Nature.* **431**, 707–712 (2004).
29. Turner, N. C. *et al.* A synthetic lethal siRNA screen identifying genes mediating sensitivity to a PARP inhibitor. *The EMBO journal.* **27**, 1368–1377 (2008).
30. Hegi, M. E. *et al.* MGMT gene silencing and benefit from temozolomide in glioblastoma. *The New England journal of medicine.* **352**, 997–1003 (2005).
31. Butowski, N. *et al.* Phase II and pharmacogenomics study of enzastaurin plus temozolomide during and following radiation therapy in patients with newly diagnosed glioblastoma multiforme and gliosarcoma. *Neuro-oncology.* **13**, 1331–1338 (2011).
32. Zahreddine, H. A. *et al.* The sonic hedgehog factor GLI1 imparts drug resistance through inducible glucuronidation. *Nature.* **511**, 90–93 (2014).
33. Gruber Filbin, M. *et al.* Coordinate activation of Shh and PI3K signaling in PTEN-deficient glioblastoma: new therapeutic opportunities. *Nature medicine.* **19**, 1518–1523 (2013).
34. Pfaffl, M. W. A new mathematical model for relative quantification in real-time RT-PCR. *Nucleic acids research.* **29**, e45 (2001).
35. Maitra, A. *et al.* Mutational landscape of gingivo-buccal oral squamous cell carcinoma reveals new recurrently-mutated genes and molecular subgroups. *Nature communications.* **4**, 2873 (2013).
36. Benjamini, Y. H. Yosef Controlling the false discovery rate: a practical and powerful approach to multiple testing. *Journal of the Royal Statistical Society.* **57**, 289–300 (1995).

Acknowledgments

We thank all the patients and patient families for their kind cooperation and constant support. We are thankful to Dr. Gregory Riggins at the Johns Hopkins University School of Medicine, Baltimore, MD, USA for his valuable suggestions while developing the neurospheres in our laboratory. We are especially grateful to Dr. Carrie L. Iwema, University of Pittsburgh, PA, USA for carefully reviewing this manuscript. We acknowledge Dr. Samsiddhi Bhattacharjee, NIBMG, India, for the fruitful discussions in developing statistical methods. We thank Biswanath Bhattacharya, NIBMG, Sarita Misra, AMRI hospitals, and Subhro Majumder, Medica Superspecialty Hospital, for helping with patient records and following up patients in clinic. We acknowledge Prof. Sharmila Sengupta and Ms. Paramita Mandal, NIBMG, for helping us with IHC experiments, Dr. Sandeep Singh, NIBMG for helping us with flow cytometry experiments. We acknowledge the members of NIBMG DNA sequencing and Microarray laboratories. We thank Prof. Partha P. Majumder, Director, NIBMG, for all the fruitful academic discussions and also for supporting us with institutional funds.

Author contributions

The senior (last) author S.D. conceived the idea, designed the study, performed the lead experiments to develop the model system in the laboratory and wrote the manuscript with inputs from other authors. V.C. performed the *in vitro* experiments of annexin V, CFSE and qRT-PCR; N.K.B. developed the pipeline of analysis of NGS data along with A.M., S.K. and S.D. (co-first authors N.K.B and V.C. equally contributed to the work). N S.R. performed the SNP-Chip microarray experiments and analysed the data; R.N.B., L.N.T. and S.K.B. performed the intracranial surgeries and helped with the clinical data; T.D. did the Immunofluorescence staining experiments; T.D. along with A.C. and P.B. did the experiments with MGMT; A.M. led the NGS library preparation and sequencing experiments; A.B. and A.M. helped with all the statistical analyses and with the design of the NGS analyses; A.C. helped with IPA. All authors have critically reviewed and approved the final manuscript in the present form.

Additional information

Accession number for data submission to European Nucleotide Archive (ENA): Study accession number is PRJEB4923. Secondary study accession number is: ERP004260. Study unique name is: ena-STUDY-NIBMG-06-11-2013-06:41:03:355-125. The URL to study accession is http://www.ebi.ac.uk/ena/data/view/PRJEB4923

Supplementary information accompanies this paper at http://www.nature.com/scientificreports

Competing financial interests: The authors declare no competing financial interests.

This work was carried out by an intramural funding support from NIBMG, India.

How to cite this article: Biswas, N.K. *et al.* Variant allele frequency enrichment analysis *in vitro* reveals sonic hedgehog pathway to impede sustained temozolomide response in GBM. *Sci. Rep.* **5**, 7915; DOI:10.1038/srep07915 (2015).